

1 **The Formulation and Atmospheric Simulation**  
2 **of the Community Atmosphere Model: CAM3**

3 **William D. Collins<sup>1\*</sup>, Philip J. Rasch<sup>1</sup>, Byron A. Boville<sup>1</sup>, James J. Hack<sup>1</sup>,**  
**James R. McCaa<sup>1</sup>, David L. Williamson<sup>1</sup>, Bruce Briegleb<sup>1</sup>,**  
**Cecilia Bitz<sup>2</sup>, Shian-Jiann Lin<sup>3</sup>, and Minghua Zhang<sup>4</sup>**

<sup>1</sup> National Center for Atmospheric Research, Boulder, Colorado 80307

<sup>2</sup> University Of Washington, Seattle, Washington 98105

<sup>3</sup> Geophysical Fluid Dynamics Laboratory, Princeton, New Jersey 08542

<sup>4</sup> Stony Brook University, Stony Brook, New York 11794

4 December 6, 2004

5 **Abstract**

6 A new version of the Community Atmosphere Model (CAM) has been  
7 developed and released to the climate community. CAM3 is an atmo-  
8 spheric general circulation model that includes the Community Land Model  
9 (CLM3), a slab-ocean model, and a thermodynamic sea-ice model. The  
10 dynamics and physics in CAM3 have been substantially changed com-  
11 pared to implementations in previous versions. CAM3 includes finite-  
12 volume dynamics in addition to Eulerian spectral and semi-Lagrangian  
13 formulations. It supports coupled simulations using either finite-volume  
14 or Eulerian dynamics through an explicit set of adjustable parameters gov-  
15 erning the model time step, cloud parameterizations, and condensation  
16 processes. The model includes separate prognostic equations for cloud  
17 water and cloud ice. The condensate is affected by advection, sedimenta-  
18 tion, and detrainment from shallow and frontal convection. Snow and rain  
19 are formed explicitly by the parameterizations for precipitation processes.  
20 The radiative parameterizations have new treatments of the interactions  
21 among water vapor, aerosols, and shortwave and longwave radiation. The  
22 effects of cloud geometry on radiative processes are calculated using a  
23 novel treatment of cloud overlap. The model includes a climatology for  
24 sulfate, soil dust, sea salt, carbonaceous, and volcanic aerosol species.  
25 These changes have improved several aspects of the simulated climate,  
26 including more realistic tropical tropopause temperatures, boreal winter  
27 land-surface temperatures, surface insolation, and clear-sky surface radia-  
28 tion in polar regions. The variation of cloud radiative forcing during ENSO

---

\*NCAR, P.O. Box 3000, Boulder, CO. 80307, email: wcollins@ucar.edu

29 events exhibits much better agreement with satellite observations. Despite  
30 these improvements, several systematic biases reduce the fidelity of the  
31 simulations. These biases include underestimation of tropical variability,  
32 errors in tropical oceanic surface fluxes, underestimation of implied ocean  
33 heat transport in the southern hemisphere, excessive surface stress in storm  
34 tracks, and offsets in the 500mb height field and Aleutian low.

## 35 1. Introduction

36 The Community Atmosphere Model (CAM3) represents the sixth generation of atmo-  
37 spheric general circulation models (AGCMs) developed by the climate community in  
38 collaboration with the National Center for Atmospheric Research (NCAR). Like its  
39 predecessors, CAM is designed to be a modular and versatile model suitable for cli-  
40 mate studies by the general scientific community (Collins et al. 2004c). CAM3 can  
41 be run either as a stand-alone AGCM or as a component of the Community Climate  
42 System Model (CCSM) (Collins et al. 2004a). In its stand-alone mode, CAM3 is in-  
43 tegrated together with the Community Land Model (Bonan et al. 2002; Oleson et al.  
44 2004), a thermodynamic sea ice model, and an optional slab-ocean model (Hack et al.  
45 2004a)<sup>1</sup>. In its coupled mode, CAM3 is integrated together with the CLM, the Com-  
46 munity Sea-Ice Model (CSIM5) (Briegleb et al. 2004), and the Parallel Ocean Program  
47 (POP). The stand-alone mode is particularly suitable for examining the response of  
48 the atmospheric circulation and state to observed patterns and changes in sea-surface  
49 temperature. It can also be used to estimate the equilibrium response to external forc-  
50 ings, for example anthropogenic increases in atmospheric carbon dioxide. The coupled  
51 model is suitable to studying the interactions of the atmosphere, ocean, cryosphere, and  
52 land surface on seasonal to millennial timescales.

53 The first four versions were in a series of Community Climate Models (CCM)  
54 starting with CCM0 (Washington 1982; Williamson 1983), continuing with CCM1  
55 (Williamson et al. 1987) and CCM2 (Hack et al. 1993), and ending with CCM3 (Kiehl  
56 et al. 1998). CCM3 was the first version with the flexibility to run either as a standalone  
57 AGCM or as a component of a coupled Climate System Model (CSM1) (Boville and  
58 Gent 1998). This change in the functionality prompted several changes in nomencla-  
59 ture. After the release of CCM3 and CSM1, the developers decided to rename the  
60 AGCM as the Community Atmosphere Model (CAM) and the coupled framework as  
61 the Community Climate System Model (CCSM). CAM2 and CCSM2 were released  
62 to the climate community in May 2002 (Kiehl and Gent 2003). It soon became evi-  
63 dent that CCSM2 and stand-alone CAM2 exhibited a number of systematic biases that  
64 needed to be addressed to improve the fidelity of climate simulations. These include  
65 high boreal winter land-surface temperatures, low tropical tropopause temperatures, bi-  
66 ases in surface fluxes in coastal stratus regions, relatively weak tropical variability, and  
67 errors in the structure of the inter-tropical convergence zones (ITCZs). After another  
68 cycle of analysis and development, CCSM3 and CAM3 were released to the climate  
69 community in June 2004. As we will show, the development effort succeeded in reduc-  
70 ing several of these biases. The comparisons are based upon stand-alone integrations

---

<sup>1</sup>line 45: What should replace Hack/Bitz 2004 SOM reference?

71 of CAM using Eulerian spectral dynamics with T85 spectral truncation for CAM3 and  
72 T42 truncation for earlier versions. The implementation of CAM3 with T85 spectral  
73 dynamics is the version used in simulations with CCSM3 for international climate-  
74 change assessments.

75 This paper will discuss the new physics and dynamics of CAM3, summarize ba-  
76 sic aspects of the climate simulation, and describe and analyze some of the improve-  
77 ments in the climate simulation relative to previous versions. The properties include  
78 the global energetics, thermodynamic profiles, global and zonal-mean characteristics of  
79 the hydrological cycle, and meridional transports of heat and moisture. The mean state  
80 and transient behavior of the simulated hydrological cycle are discussed in Hack et al.  
81 (2004b) and Rasch and Etcetera (2004), and the dynamic circulation is described in  
82 Hurrell and Etcetera (2004). Other aspects of the atmospheric simulation and improve-  
83 ments in the simulation fidelity are discussed in the overview of CCSM3 by Collins  
84 et al. (2004a). It is important to note that some of the changes in the climate simulation  
85 are related to the change in land-surface model. The changes related to improvements  
86 in CLM are discussed by Bonan et al. (2002).

87 The new formulations of physics and dynamics are outlined in section 2. A more  
88 complete technical description of the physical basis and numerical implementation of  
89 these changes is given in Collins et al. (2004c). The mean features of the atmospheric  
90 state, energetics, and energy transport are presented in section 3. The reduction in  
91 model biases relative to previous versions are discussed in section 4. Several of the  
92 main biases remaining in the climate simulation from CAM3 and the methods under  
93 consideration for reducing them are described in section 5, followed by conclusions in  
94 section 6.

## 95 **2. Overview of new physics and dynamics**

### 96 **a. Dynamical frameworks**

97 Previous versions of CAM have included Eulerian spectral and semi-Lagrangian dy-  
98 namics. CAM3 includes the finite volume (FV) dynamical core developed by Lin and  
99 Rood (1996), and its initial applications include simulations of atmospheric chemical  
100 transport and chemical processes (Boville et al. 2004; Rasch 2004). The physical pa-  
101 rameterizations have been separated from the dynamical core, and the dynamics can  
102 be coupled to the physics in a time-split or process-split approximation (Williamson  
103 2002). In the process-split technique, the calculations of dynamical and physical ten-  
104 dencies for prognostic variables are based upon the same past state. In the time-split  
105 technique, the tendencies for dynamics and physics are computed sequentially, each  
106 based upon the state produced by the other. In CAM3, all process are time split by  
107 default.<sup>2</sup>

108 CAM3 has been designed to produce simulations with reasonable fidelity for sev-  
109 eral different dynamical cores and horizontal resolutions. In the absence of any mod-  
110 ifications to the physical parameterizations, changes in resolution and dynamics both  
111 introduce perturbations in the mean climate and the top-of-atmosphere (TOA) energy

---

<sup>2</sup>line 107: Is it true that all processes are time split by default in CAM3?

112 balance of CAM3. In order to run CAM3 as part of a stable coupled system, the energy  
113 balance has been restored by adjusting twelve parameters governing cloud condensate,  
114 cloud amount, and precipitation processes (Collins et al. 2004c). The model time step  
115 is also adjusted to satisfy the Courant-Friedrichs-Levy (CFL) condition. In its current  
116 implementation, the adjustable parameters have been configured for the Eulerian dy-  
117 namical core at T31, T42, and T85 spectral truncations and for the FV core at  $2^\circ \times 2.5^\circ$   
118 horizontal resolution. The Eulerian truncations correspond to zonal resolutions ranging  
119 from  $3.75^\circ$  for T31 to  $1.41^\circ$  for T85.

#### 120 **b. *New treatment of cloud and precipitation processes***

121 The treatments of microphysics and cloud condensate have been substantially revised  
122 in CAM3 (Boville and Etcetera 2004). The diagnostic cloud-water scheme used in  
123 CCM3 has been replaced by the prognostic cloud-water parameterization of Rasch and  
124 Kristjánsson (1998) updated by Zhang et al. (2003). The new model includes sepa-  
125 rate evolution equations for the liquid and ice-phase condensate, .The revised scheme  
126 includes a new formulation of the fractional condensation rate and a self-consistent  
127 treatment of the evolution of water vapor, heat, cloud fraction, and in-cloud condensate  
128 (Zhang et al. 2003). Condensed water detrained from shallow and frontal convection  
129 can either form precipitation or additional stratiform cloud water. Convective precipi-  
130 tation can evaporate into its environment at a rate determined from Sundqvist (1988).  
131 The latent heats of vaporization and fusion are consistently applied to transformations  
132 involving liquid and ice-phase condensate and precipitation, respectively.

133 Advection and sedimentation of loud droplets and ice particles are included in the  
134 equations governing cloud condensate. The settling velocities for liquid and ice-phase  
135 constituents are computed separately following Lawrence and Crutzen (1998). The  
136 ice effective radius used in the microphysics and radiation is a function of tempera-  
137 ture obtained from Kristjánsson and Kristiansen (2000). The effective radius and the  
138 prescribed number density of liquid droplets transition from polluted values over land  
139 surface to pristine values over ocean. This transition affects the radiative properties and  
140 microphysical evolution of these droplets.

#### 141 **c. *Radiative processes***

142 The radiative parameterizations have been updated to include new treatments of the  
143 interactions of shortwave and longwave radiation with cloud geometry and with water  
144 vapor. The modifications to cloud overlap and longwave interactions were originally  
145 introduced in CAM2, and the shortwave absorption by water vapor has been modi-  
146 fied in CAM3. The new, generalized formulation for clouds can calculate the radiative  
147 fluxes and heating rates for any arbitrary combination of maximum and random overlap  
148 (Collins 2001b). The type of overlap is completely separated from the radiative param-  
149 eterizations, and it can vary from one grid cell or time step to the next. In practice,  
150 CAM3 applies a standard maximum-random cloud overlap scheme (Zdunkowski et al.  
151 1982) to all cloud configurations. The parameterizations are mathematically equivalent  
152 to the independent column approximation (ICA) and reproduce ICA solutions to within  
153 user-selectable limits.

154 The absorption and emission of longwave radiation by water vapor have been up-

155 dated using modern spectral line data bases and empirical approximations for the water-  
156 vapor continuum. The parameterizations for these terms have been replaced with new  
157 terms calculated using the Hitran2K line data and its 2001 update (Rothman et al. 2003)  
158 together with the CKD 2.4.1 model for the continuum based upon Clough et al. (1989).  
159 The terms are derived from line-by-line radiative calculations using the methodology  
160 of Collins et al. (2002a). These changes increase the cooling at 300 mb due to line ab-  
161 sorption and the foreign continuum in the rotation band, and they decrease the cooling  
162 near 800 mb due to the self-continuum in the rotation band. The changes in the verti-  
163 cal profile of longwave cooling interact with the parameterized convection in a manner  
164 consistent with the theory of radiative-convective equilibrium.

165 The absorption of near-infrared radiation by water vapor has been updated using  
166 the same modern line data and approximation for the continuum (Collins et al. 2004b).  
167 The clear-sky and all-sky shortwave absorption increase by  $4.0 \text{ Wm}^{-2}$  and  $3.1 \text{ Wm}^{-2}$ ,  
168 respectively, in calculations replacing the old with the new spectroscopic parameters.  
169 The main changes in the water-vapor spectroscopy responsible for the increased ab-  
170 sorption are the addition of many missing weak lines and increased estimates of line  
171 strength. The atmosphere becomes warmer, moister, and more stable with the increased  
172 absorption.

#### 173 **d.** *Atmospheric aerosols*

174 In its default configuration, CAM3 includes the radiative effects of an aerosol climatol-  
175 ogy in its calculation of shortwave fluxes and heating rates. This climatology replaces  
176 the globally uniform sulfate aerosol distribution used in previous versions of CCM  
177 (Kiehl et al. 1996). The new aerosol data set includes the annually-cyclic, monthly-  
178 mean distributions of sulfate, sea-salt, carbonaceous, and soil-dust aerosols. The cli-  
179 matology is derived from a chemical transport model constrained by assimilation of  
180 satellite retrievals of aerosol depth (Collins et al. 2001; Rasch et al. 2001). The clima-  
181 tology in CAM3 is obtained from an aerosol assimilation for the period 1995–2000.  
182 The effects of the aerosols on the shortwave fluxes and heating rates are calculated fol-  
183 lowing Collins et al. (2002b). In place of the sulfate climatology, the sulfate aerosols  
184 can also be predicted using the sulfur cycle of Barth et al. (2000) and Rasch et al.  
185 (2000). The effects of volcanic aerosols released by eruptions during the 19th and 20th  
186 centuries are obtained from a reconstruction by Ammann et al. (2003).

#### 187 **e.** *Slab-ocean and sea-ice models*

188 The slab ocean and sea-ice models in CAM3 are designed to emulate the surface ex-  
189 changes in the full coupled CCSM3 without incurring the computational expense of  
190 ocean and ice dynamics (Hack et al. 2004a)<sup>3</sup>. These models are frequently used to  
191 estimate the equilibrium response to external forcings, for example increased concen-  
192 trations of carbon dioxide or anthropogenic aerosols. The heat content in the slab ocean  
193 is represented by a single temperature. Internal ocean heat exchange and ocean trans-  
194 port are emulated using a surface flux obtained from an equilibrium control simulation.

195 CAM3 includes a revised thermodynamic sea-ice model that uses much of the same

---

<sup>3</sup>line 190: What should replace Hack/Bitz 2004 SOM reference?

196 physics as the full dynamic sea-ice model CSIM5 in CCSM3 (Hack et al. 2004a)<sup>4</sup>. The  
197 thermodynamic model simulates the snow depth, surface temperature, ice thickness,  
198 ice fractional coverage, and energy exchange in a four-layer representation of the sea  
199 ice. It is designed to operate in two modes governed by the source of sea-surface  
200 temperatures. If sea surface temperatures (SSTs) are obtained from a boundary data  
201 set, then ice coverage and ice thickness are also input from a data set. In this case,  
202 the sea-ice model is just used to compute energy fluxes between the ice and overlying  
203 atmosphere. If the SSTs are computed using the slab-ocean model, the ice coverage  
204 and thickness are calculated by the sea-ice model.

205 **f. Heating, kinetic Energy Dissipation, and vertical diffusion**

206 The calculation of thermodynamic tendencies has been reformulated to insure conser-  
207 vation of energy (Boville and Bretherton 2003). Dry static energy is predicted by each  
208 physical parameterization and is updated following each parameterization. The evolu-  
209 tion of the temperature and geopotential are then efficiently obtained from the updated  
210 dry static energy. The dissipation of kinetic energy from vertical diffusion of momen-  
211 tum is calculated explicitly and included in the heating applied to the atmosphere. The  
212 parameterization for vertical diffusion has been also generalized to include molecular  
213 diffusion above the mesopause and to permit diffusive separation of constituents of dif-  
214 ferent molecular weights. The standard version of CAM3 applies identical molecular  
215 viscosities and diffusivities to all atmospheric gases in the upper atmosphere.

216 **g. Boundary data for orography, sea-ice extent, and sea-surface temperatures**

217 The data sets used for sea-surface temperature, sea-ice concentration, and sub-grid oro-  
218 graphic variations have been replaced with new versions in CAM3. The sea-surface  
219 temperatures and sea-ice concentrations are used in stand-alone integrations of the  
220 CAM3. These datasets prescribe analyzed monthly mid-point mean values of SST and  
221 ice concentration for the period 1950 through 2001. The dataset is a blended product,  
222 using the global HadISST OI dataset prior to 1981 and the Smith/Reynolds EOF dataset  
223 post-1981<sup>5</sup>. These are the data used in the ensemble of T85 integrations analyzed in  
224 this paper.<sup>6</sup>

225 **3. Basic properties of the simulated climate and general**  
226 **circulation**

227 The analysis of CAM3 is based upon the average of a 5-member ensemble integrated  
228 at T85 resolution using observed sea-surface temperatures (section 2.g) from 1950 to  
229 2000. In these runs, the concentrations of greenhouse gases are held constant at 1990  
230 levels, and the concentrations of aerosols are obtained from a present-day climatology

<sup>4</sup>line 196: What should replace Hack/Bitz 2004 SOM reference?

<sup>5</sup>line 223: Insert reference here to Hack/Hurrell paper on new SST datasets

<sup>6</sup>line 224: What is the source of the sub-grid orography used by default in CAM3? What are the appropriate references?

231 (section 2.d). The period analyzed here corresponds to the portion of the satellite data  
232 record from 1980 through 2000.

233 The global annual average properties of the simulation are given in Table 1.<sup>7 8</sup> The  
234 most significant changes in the shortwave energy budget from CAM2 to CAM3 are re-  
235 lated to changes in aerosols, extinction by water vapor, cloud amount, and cloud water  
236 path. The increase of  $5.2 \text{ Wm}^{-2}$  in clear-sky TOA absorbed shortwave flux is due pri-  
237 marily to the switch from a uniform background aerosol to a more detailed climatology  
238 with multiple aerosol species. The albedo of the aerosols in the climatology is less than  
239 the albedo of the background aerosol. The reduction by  $1.9 \text{ Wm}^{-2}$  in clear-sky surface  
240 insolation is caused by the increased atmospheric absorption of shortwave radiation  
241 related to the greater extinction by water vapor and to the introduction of absorptive  
242 aerosol species. The magnitude of shortwave cloud forcing is greater by  $5.9 \text{ Wm}^{-2}$   
243 in CAM3 despite a reduction in total cloud amount from 60.7% in CAM2 to 56.1%  
244 in CAM3. One reason for the increased cloud albedo is the shift in the vertical cloud  
245 distributions, with 13.8% lower high cloud cover and 8.5% greater low cloud cover. In  
246 CAM3, the mean optical thickness of low clouds are larger than the optical thickness of  
247 high clouds. In addition, the global mean cloud water path in CAM3 is approximately  
248 two times larger than the cloud water path in CAM2.

249 The changes to the infrared absorption and emission by water vapor in CAM3 in-  
250 crease the downwelling longwave flux at the surface and the upwelling flux at TOA<sup>9</sup>  
251 (Collins et al. 2002a). As a result of these effects and the decrease in surface mean  
252 temperature by 0.73K, the net all-sky and clear-sky surface longwave fluxes decrease  
253 by  $6.1$  and  $6.3 \text{ Wm}^{-2}$ , respectively. The longwave cloud radiative effects at TOA in-  
254 crease by  $1.4 \text{ Wm}^{-2}$  and the effects at the surface decrease by  $0.2 \text{ Wm}^{-2}$  despite the  
255 large changes in the vertical distribution of cloud and the doubling of the global mean  
256 cloud water path.

257 The global mean statistics of the hydrological cycle are nearly identical between  
258 the two models. The precipitable water increases by 1.7%, the latent heat flux by 1.1%,  
259 and the 0.3% from CAM2 to CAM3. The zonal mean difference between evapora-  
260 tion and precipitation, which measures the net exchange of water between the surface  
261 and atmosphere, is nearly identical<sup>10</sup> The major change between the two models is a  
262 reduction in the precipitation in the southern branch of the tropical ITCZ. The zonal  
263 mean precipitation at 5S decreases by 1 mm/day, and the precipitation on the equator  
264 increases by 0.6 mm/day<sup>11</sup>. Compared against the GPCP estimates, CAM3 overes-  
265 timates the precipitation in the tropics between 25N to 25S by 0.6 mm/day<sup>12</sup> CAM3  
266 underestimates the subtropical precipitation between 30N–40N by 0.4 mm/day and be-  
267 tween 30S–40S by 0.3 mm/day<sup>13</sup> Further analysis of the mean hydrological cycle in  
268 CAM3 is presented in Hack et al. (2004b).

269

<sup>7</sup>line 233: What is the reference for Trenberth-modified ERBE.

<sup>8</sup>line 233: ISCCP cloud amounts do not add up to  $\geq$  total cloud amount – doesn't make sense

<sup>9</sup>line 250: Confirm against tables in CHE paper.

<sup>10</sup>line 261: Quantify differences in zonal-mean  $E - P$  between CAM2 and CAM3.

<sup>11</sup>line 264: Quantify changes in zonal mean precipitation from CAM2 to CAM3.

<sup>12</sup>line 265: What is the mean difference between CAM3 and GPCP for 25S–25N.

<sup>13</sup>line 267: What are the differences between CAM3 and GPCP for 30N–40N and 30S–40S.

Table 1

Table 1: Global annual-mean climatological properties of CAM2 and CAM3

Property	CAM2	CAM3	Observation
TOA Outgoing longwave radiation ( $\text{Wm}^{-2}$ , + upwards)			
all sky	235.5	235.6	234.0 <sup>a</sup>
clear sky	264.9	266.2	264.4 <sup>a</sup>
TOA Absorbed solar radiation ( $\text{Wm}^{-2}$ , + downwards)			
all-sky	237.7	237.1	234.0 <sup>a</sup>
clear-sky	286.5	291.7	289.3 <sup>a</sup>
Longwave cloud forcing ( $\text{Wm}^{-2}$ )	29.3	30.7	30.4 <sup>a</sup>
Shortwave cloud forcing ( $\text{Wm}^{-2}$ )	-48.8	-54.7	-54.2 <sup>a</sup>
Cloud fraction (%)			
total	60.7	56.1	66.7 <sup>b</sup>
low	31.6	40.1	28.0 <sup>b</sup>
medium	19.1	17.3	20.0 <sup>b</sup>
high	43.1	29.3	13.0 <sup>b</sup>
Cloud water path (mm)	0.060	0.122	0.112 <sup>c</sup>
Precipitable water (mm)	23.9	24.3	24.6 <sup>d</sup>
Latent heat flux ( $\text{Wm}^{-2}$ )	82.9	83.8	84.9 <sup>e</sup>
Sensible heat flux ( $\text{Wm}^{-2}$ )	20.0	17.8	15.8 <sup>f</sup>
Precipitation (mm/day)	2.86	2.87	2.61 <sup>g</sup>
Net surface longwave radiation ( $\text{Wm}^{-2}$ , + upwards)			
all-sky	64.1	58.0	49.4 <sup>h</sup>
clear-sky	92.1	85.8	78.7 <sup>h</sup>
Net surface shortwave radiation ( $\text{Wm}^{-2}$ , + downwards)			
all-sky	167.7	159.1	165.9 <sup>h</sup>
clear-sky	220.5	218.6	218.6 <sup>h</sup>
Annual mean budgets ( $\text{Wm}^{-2}$ , + upwards)			
TOM	0.45	-0.44	
Surface	0.68	-0.47	

<sup>a</sup> ERBE

<sup>b</sup> ISCCP (Rossow and Schiffer 1999)

<sup>c</sup> MODIS (King et al. 2003)

<sup>d</sup> NVAP (Randel et al. 1996)

<sup>e</sup> ECMWF (Källberg et al. 2004)

<sup>f</sup> NCEP (Kistler et al. 2001)

<sup>g</sup> GPCP (Adler et al. 2003)

<sup>h</sup> ISCCP FD (Zhang et al. 2004)

270 The annual implied northward heat transports for CAM2 and CAM3 are shown in  
271 Figure 1. At each latitude, these transports represent the amount of energy that the  
272 ocean, sea ice, and land must transport northward in order to balance the total heat  
273 exchanged with the atmosphere between that latitude and the north pole. In CAM3, the  
274 northward heat transport increases by 0.4–0.7 PW between the tropics and 50N. The  
275 primary reason is the reduced surface insolation in the new model. Between 5S and 5N  
276 where the the transport increase by 0.69 PW, the effects of the reduced insolation are 2.2  
277 times larger than the changes in other surface fluxes combined. Although the shortwave  
278 cloud radiative effects have increased in this region, 71% of the insolation effect is  
279 related to the increased absorption by aerosols and water vapor. Like CAM2, CAM3  
280 underestimates the southward transports in the southern hemisphere. The maximum  
281 error is approximately 1 PW at 10S.

Figure 1

#### 282 **4. Improvements in the climate simulation and reduc-** 283 **tion in model biases**

284 The differences in the physics and dynamics between CAM2 and CAM3 have helped  
285 reduce some of the more serious systematic errors in the atmospheric simulations. The  
286 improvements in the boreal winter land-surface temperatures, surface insolation, and  
287 clear-sky surface radiation in polar regions are discussed in greater detail by Collins  
288 et al. (2004a). The focus here is on aspects of the mean climate and its seasonal varia-  
289 tions.

##### 290 **a. Temperatures in the upper tropical troposphere**

291 The temperatures for the upper tropical troposphere produced by CAM3 are larger by  
292 between 2 and 4K compared to the temperatures in CAM2. The heating occurs in  
293 a large region spanning the tropopause between 70 and 150mb and between 30S to  
294 30N. The increased temperatures are in better agreement with the ECMWF and NCEP  
295 meteorological reanalysis (Kållberg et al. 2004; Kistler et al. 2001). The maximum  
296 cold bias relative to both reanalyses is now between 4 and 5K at approximately 70mb  
297 on the equator. The larger cold bias produced by CAM2 has hampered modeling the  
298 exchange of water vapor with the stratosphere because of the rising air just below the  
299 tropopause has been unrealistically supersaturated.

##### 300 **b. Spatial structure of tropical precipitation**

301 Two aspects of the simulated precipitation have improved in CAM3 compared to CAM2.  
302 The double ITCZ in the Pacific is weaker in CAM3, and the precipitation is concen-  
303 trated north of the equator as observed. In addition, the rainfall over some tropical  
304 continental areas has increased, particularly over several important rain-forest regions.

305 The secondary peak in tropical precipitation south of the equator is much weaker  
306 than the northern peak in the annual mean in the annual and JJA means in CAM3  
307 (Figure 2). The differences between the peak zonal-mean tropical precipitation in the  
308 northern hemispheres and southern hemispheres are shown in Table 2. It is evident

Figure 2

Table 2

Table 2: Difference in zonal-mean precipitation maxims<sup>a</sup>(mm/day)

Period	CAM2	CAM3	GPCP <sup>b</sup>
Annual	1.1	1.6	1.6
DJF	0.9	0.9	-0.7
JJA	1.6	3.2	4.2

<sup>a</sup> The difference in terms of the zonal-mean precipitation as the maximum value between 0N–10N minus the maximum value between 10S–0S.

<sup>b</sup> Adler et al. (2003)

309 from the table that CAM3 produces a more realistic inter-hemispheric gradient in trop-  
 310 ical precipitation than CAM2 for these time periods. However, CAM3 and CAM2 both  
 311 produce stronger precipitation in the northern branch of the ITCZ during JJA, contrary  
 312 to observations.

313

314 While CAM3 and CCSM3 still underestimate the precipitation for some mid-latitude  
 315 regions (Collins et al. 2004a), the rainfall over the Amazonian basin is now closer to  
 316 observational estimates. For this comparison, the greater Amazon basin is the region  
 317 10S–0S, 80W–50W. The annual amounts of precipitate produced by CAM2 and CAM3  
 318 are 81% and 92% of the GPCP estimate. During the higher rainfall in JJA, the precip-  
 319 itation produced by CAM2 and CAM3 are 54% and 74% of the GPCP value. The  
 320 improved fidelity of the tropical continental precipitation is important for simulations  
 321 including dynamic vegetation (Levis et al. 2004; Levis and Bonan 2004) and the ter-  
 322 restrial carbon cycle.

323 **c. Radiative effects of tropical clouds**

324 The cloud systems in the tropics are generally extensive, optically thick, and vertically  
 325 distributed from the surface to the upper troposphere. As a result, these systems can  
 326 reflect a significant fraction of incident sunlight and absorb a large fraction of the ter-  
 327 restrial radiation. Despite the large magnitudes of the shortwave and longwave cloud  
 328 radiative effects, the net effect of these systems is frequently near zero (Ramanathan  
 329 et al. 1989; Cess et al. 2001). The cancellation implies that the shortwave and long-  
 330 wave cloud radiative effects should be linearly correlated with a slope close to  $-1$ ,  
 331 and this behavior is usually observed in satellite observations. The statistics for the  
 332 cloud radiative forcing for the Indonesian region (10S–20N, 110E–160E) are given in  
 333 Table 3. Compared to ERBE, CAM2 underestimates the correlation of shortwave and  
 334 longwave cloud radiative effects in all seasons examined. It also significantly underes-  
 335 timates the range of shortwave cloud radiative forcing. The statistics for CAM3 are in  
 336 better agreement with the ERBE observations. The correlations increase in all seasons,  
 337 and the range of shortwave cloud forcing is slightly overestimated. The response of  
 338 the shortwave cloud forcing to the warming of the mid-Pacific during recent ENSOs is  
 339 also much more realistic in CAM3 (not shown).

Table 3

340

Table 3: Indonesian Cloud Forcing Statistics

Period	CAM2		CAM3		ERBE <sup>a</sup>	
	$\rho^b$	$s^c$	$\rho$	$s$	$\rho$	$s$
Annual	-0.84	-0.65	-1.24	-0.81	-1.10	-0.94
DJF	-0.49	-0.61	-1.06	-0.89	-1.05	-0.93
JJA	-0.79	-0.74	-0.98	-0.82	-1.00	-0.96

<sup>a</sup> citation

<sup>b</sup>  $\rho$  is the Pearson correlation coefficient.

<sup>c</sup>  $s$  is the linear least-squares slope for SWCF vs LWCF.

341 **d. The 200mb height field**

342 The improvements in CAM3 can be quantified using a skill score for climate models  
 343 (Williamson 1995) based upon fidelity of the simulated 200-mb height field. The same  
 344 score was applied to CCM3 and its preceding versions (Kiehl et al. 1998). It is a func-  
 345 tion of the height  $z_m$  produced by the model and the height  $z_a$  from a meteorological  
 346 analysis. A perfect score of 0 indicates that the model is able to reproduce the exact  
 347 spatial pattern of the 200-mb height field in the analysis. Let  $s_m$  and  $s_a$  represent the  
 348 spatial variances of the modeled and analyzed height fields. Let an overbar denote an  
 349 area average over the domain of interest. Then the score is given by a scaled variance  
 350 ratio (SVR)

$$\text{SVR}(z_m) = \left( \frac{s_m}{s_a} \right)^2 \text{NMSE}(z_m) \quad (1)$$

$$\text{NMSE}(z_m) = (z_m - \bar{z}_a)^2 / (z_a - \bar{z}_a)^2 \quad (2)$$

351 where NMSE is the normalized mean square error. The NMSE can be rewritten as a  
 352 sum of three non-negative terms as:

$$\text{NMSE}(z_m) = U(z_m) + C(z_m) + P(z_m) \quad (3)$$

353 The first term  $U(z_m)$  is a measure of the unconditional bias in the model, and it van-  
 354 ishes only if the average model and analyzed heights are equal. The second term  $C(z_m)$   
 355 is a measure of the conditional bias in the model. It vanishes if linear regressions of  
 356 the analyzed heights against the modeled heights yield slopes equal to unity. The third  
 357 term  $P(z_m)$  is a measure of phase errors and vanishes if the model and analysis fields  
 358 are perfectly linearly correlated.

359 These scores have been computed for the 200-mb height field during January in the  
 360 northern hemisphere. The results are displayed in Figure 3 for each version of CCM  
 361 and CAM. The results show that the SVR, NMSE, and unconditional error  $U(z_m)$  have  
 362 declined with each successive version of CCM and CAM. The scores for CAM3 at T85  
 363 truncation are the lowest of any of the models. However, this version has slightly higher  
 364 conditional and phase errors than CCM3. This graph illustrates the steady improvement  
 365 in the simulation of the atmosphere in the CCM/CAM series.

Figure 3

## 366 5. Challenges for future development

367 Despite the improvements in the climate simulation produced by CAM3, there are  
368 still many significant challenges for future development. Issues with the implied heat  
369 transport, particularly in the southern hemisphere, are discussed in section 3. Several  
370 of the model deficiencies are discussed in the context of the CCSM3 integrations in  
371 Collins et al. (2004a), including:

- 372 • biases in mid-latitude continental precipitation and surface temperature;
- 373 • errors in the radiative fluxes and surface stress in western coastal regions; and
- 374 • underestimation of downwelling shortwave radiation in polar regions.

375 For the sake of brevity, the following discussion clearly cannot be comprehensive, but  
376 it does serve to illustrate some problems in the climate simulations under investigation.

### 377 a. *The Madden-Julian oscillation*

378 Like its previous versions, CAM3 underestimates the variability associated with the  
379 Madden-Julian Oscillation (MJO). This variability can be quantified from a time series  
380 of daily 200 hPa zonal wind averaged over 10S–10N. The time series is band-pass  
381 filtered for period of 20-100 days, an a MJO index is defined as the running 101-day  
382 variance of the band-pass filtered data. The MJO indices from the NCEP reanalysis  
383 (Kistler et al. 2001) and one T85 ensemble member clearly show higher variance in the  
384 NCEP reanalysis Figure 4. A power-spectrum/histogram analysis shows . . .<sup>14</sup>

Figure 4

### 385 b. *Energy budget of the western Pacific warm pool*

386 The ability of the atmospheric model to produce a reasonable energy budget for the  
387 tropical western Pacific warm pool has important implications for the coupled simu-  
388 lation of the Pacific basin (Kiehl 1998; Collins 2001a). Previous versions of CAM  
389 and CCM significantly overestimate the annual mean surface insolation over the warm  
390 pool. When the atmosphere is coupled to CCSM, this bias is compensated by latent  
391 heat fluxes much larger than the *in situ* estimates. The reason is that the ocean dynam-  
392 ical transport out of the warm pool is limited to less than approximately  $20 \text{ Wm}^{-2}$ ,  
393 so large net radiation inputs to the ocean must be balanced by other fluxes. The TOA  
394 and surface energy budgets for CAM2 and CAM3 are compared against observations  
395 in Table 4. The table shows that the estimate of the net surface energy budget in CAM3  
396 is only  $6 \text{ Wm}^{-2}$  greater than observed, while the net budget from CAM2 is  $24 \text{ Wm}^{-2}$   
397 greater than observed. The lower CAM3 energy budget is due to a  $30 \text{ Wm}^{-2}$  reduction  
398 in surface insolation, which is partially compensated by decreases in the other fluxes.  
399 While the surface insolation in CAM3 is in better agreement with observations (Waliser  
400 et al. 1996, e.g.),  $23 \text{ Wm}^{-2}$  of the reduction is attributable to an overestimate of the  
401 TOA shortwave cloud radiative effect compared to ERBE. The remaining  $7 \text{ Wm}^{-2}$  of  
402 the reduction is caused by the increased absorption of near-infrared radiation by wa-  
403 ter vapor in CAM3 (Collins et al. 2004b). The fact that the model is unable to match

Table 4

<sup>14</sup>line 384: Complete this section once the variability analysis for the VAMIP T85 ensemble is complete.

Table 4: Warm Pool Energy Budgets (10S–10N, 140E–170E) ( $\text{Wm}^{-2}$ )

level	Flux	CAM2	CAM3	Observation <sup>a</sup>
TOA	S	317	294	309
	S <sub>clr</sub>	373	381	373
	F	−230	−212	−225
	F <sub>clr</sub>	−279	−282	−285
Surface	S	228	198	182
	S <sub>clr</sub>	287	288	282
	F	−50	−48	−49
	LH	−122	−118	−107 <sup>b</sup>
	SH	−13	−9	−8 <sup>b</sup>
	NET	42	24	18

<sup>a</sup> Collins (2001a)

404 the TOA and surface all-sky shortwave fluxes simultaneously remains a basic research  
 405 issue for future study. It should be noted that zonal-mean TOA cloud radiative ef-  
 406 fects are also overestimated for the entire tropics, particularly the northern branch of  
 407 the Hadley cell.

408

409 **c. Surface stress in the storm tracks**

410 CAM3 simulates larger surface stresses than observed in the storm tracks in both hemi-  
 411 sphere. The biases appear throughout the annual cycle, so for simplicity consider a  
 412 comparison of the annual mean stress from CAM3 and the European Remote Sensing  
 413 Satellite (ERS) scatterometer <sup>15</sup> The excess stress occurs in the southern Indian and  
 414 Atlantic oceans adjacent to the Antarctic circumpolar current, the northern Atlantic be-  
 415 tween Nova Scotia and Great Britain, and the northern Pacific and Sea of Okhotsk. In  
 416 terms of zonal means, the peak errors in each hemisphere occur at 52N and 49S. At  
 417 both latitudes, the stress is too large by 0.07 N/m<sup>2</sup>. In the northern hemisphere, this  
 418 constitutes an overestimate by 144%, while in the southern hemisphere the overesti-  
 419 mate is by 56%. When the atmosphere is coupled to a dynamic ocean, these stress  
 420 errors lead to ocean mass transports larger than observed, particularly in the Drake  
 421 passage (Large et al. 2004).

422 **d. The Aleutian and Icelandic lows**

423 *Discussion . . .*

424 **6. Conclusions**

425 A new version of the Community Atmosphere Model, CAM3, has been developed  
 426 and released to the scientific community. CAM3 includes new dynamical formulations

<sup>15</sup>line 413: Need reference for ERS wind retrievals.

427 and extensive improvements to the physical parameterizations. The model produces  
428 atmospheric simulations suitable for use in a fully coupled system that includes the  
429 land surface, full-depth ocean, and dynamic sea ice. The model physics is designed  
430 to maintain the fidelity of the simulations over a wide range of spatial resolutions and  
431 multiple dynamics. This is accomplished by making the model time-step and other  
432 adjustable parameters dependent on the resolution and dynamics. The adjustable pa-  
433 rameters affect the parameterizations of cloud and precipitation processes. The version  
434 of the model documented here is based upon the Eulerian spectral dynamics with T85  
435 spectral truncation.

436 The new atmospheric model includes significant changes to the dynamics, cloud  
437 and precipitation processes, radiation processes, and treatments of aerosols. The finite  
438 volume dynamical core is now included as a standard option for integrating CAM. The  
439 tendency equations can be integrated with either process-split or time-split formula-  
440 tions of the numerical difference approximations. The physics of cloud and precip-  
441 itation processes has been modified extensively. The modifications include separate  
442 treatments of liquid and ice condensate; advection, detrainment, and sedimentation  
443 of cloud condensate; and separate treatments of frozen and liquid precipitation. The  
444 radiation has been updated with a generalized treatment of cloud geometrical over-  
445 lap and new treatment of longwave and shortwave interactions with water vapor. A  
446 prognostic sulfur cycle for predicting sulfate aerosols is now a standard option for the  
447 model. A prescribed distribution of sulfate, soil dust, carbonaceous species, and sea  
448 salt based upon a three-dimensional assimilation is used to calculate the direct effects  
449 of tropospheric aerosols on the heating rates. The model also includes the effects of  
450 stratospheric volcanic aerosols.

451 Several important features of the atmospheric simulation are improved in CAM3.  
452 The cold temperature bias at the tropical tropopause has been reduced by at least 50%<sup>16</sup>.  
453 The overestimation of boreal winter sub-Arctic land surface temperatures has been re-  
454 duced by 2 to 4K in Eurasia, the western U.S. and Canada, and Greenland. The surface  
455 precipitation over northern South America has increased from CAM2 to CAM3, al-  
456 though the model still does not produce enough rainfall over the Amazonian basin.  
457 The global annual-mean surface net insolation has been reduced by  $8.6 \text{ Wm}^{-2}$  to a  
458 value consistent with the range of empirical estimates. The clear-sky longwave fluxes  
459 in polar regions are in much better agreement with observations. The structure of the  
460 ITCZ in the tropical Pacific is more realistic, with a weaker and less zonal SPCZ and  
461 stronger rainfall in the northern portion of the tropical Pacific warm pool. The relation-  
462 ship of longwave and shortwave effects for tropical cloud systems is more consistent  
463 with satellite observations. As a result, the response of cloud radiative forcing to ENSO  
464 variations has the correct sign and spatial structure in CAM3. The seasonal cycle of  
465 shortwave cloud forcing and cloud amount is more realistic in the northern Pacific and  
466 the coastal stratus regions.

467 A number of significant challenges remain for future study and development. Like  
468 the preceding models, CAM3 does not produce a reasonable simulation of the Madden-  
469 Julian oscillation. The amplitude of the 30–90 day variability is too low<sup>17</sup>, and the wave

---

<sup>16</sup>line 452: Quantify reduction in tropopause temp. bias.

<sup>17</sup>line 469: Quantify underestimation of MJO variance.

470 trains do not consistently propagate eastward. The surface stress is much too large  
471 relative to satellite retrievals in the storm tracks, especially in the region just north of  
472 the Antarctic circumpolar current. As a result, the coupled model overestimates the  
473 mass transport through the Drake Passage by over 50%. However, the surface stresses  
474 are still weaker than observed in the coastal stratus regions west of South America and  
475 Africa. There are biases of up to 100 m in the 500 mb height field. The strength of  
476 the Aleutian low is too low and the strength of the Icelandic low is too high by roughly  
477 6 mb.

478 Future development will focus on these and other systematic errors in the atmo-  
479 spheric simulation. The development activities underway include cloud-resolving mod-  
480 els to characterize the process-level behavior of cloud systems. The model is also be-  
481 ing extended to include reactive chemistry and photochemistry from the troposphere  
482 through the thermosphere. Much more detailed treatments of the formation and evo-  
483 lution of the major aerosol species have also been brought online. The introduction  
484 of chemistry into CAM has elevated the importance of tracer transport and flux-form  
485 dynamics. Further progress in simulation fidelity will be measured in terms of both the  
486 physical and chemical state of the atmosphere.

487 **Acknowledgement** The authors wish to acknowledge members of NCAR's Climate  
488 Modeling Section, Computer Software and Engineering Group, and Scientific Com-  
489 puting Division for their contributions to the development of CAM3.

490 The new model would not exist without the significant input from members of the  
491 CCSM Atmospheric Model Working Group too numerous to mention. Bill Collins  
492 (NCAR), Leo Donner (GFDL), James Hack (NCAR), David Randall (Colorado State  
493 University), and Phil Rasch (NCAR) were the co-chairs of the AMWG during the  
494 development of CAM3.

495 We would like to acknowledge the substantial contributions to the effort to develop  
496 CAM3 from the National Science Foundation, the Department of Energy, the National  
497 Aeronautics and Space Administration, and the National Oceanic and Atmospheric  
498 Administration.

499 Computational facilities have been provided by NCAR and by DOE. NCAR is  
500 supported by NSF. The Department of Energy's Office of Science supports the CCSM  
501 program through its Biological and Environmental Research Program and the use of  
502 high performance computing as part of its Advanced Scientific Computing Research  
503 (ASCR). ASCR provides computing at the National Energy Research Center and at the  
504 Oak Ridge National Laboratory Center for Computational Science.

## 505 **References**

506 Adler, R. F., G. J. Huffman, A. Chang, R. Ferraro, P. P. Xie, J. Janowiak, B. Rudolf,  
507 U. Schneider, S. Curtis, D. Bolvin, A. Gruber, J. Susskind, P. Arkin, and E. Nelkin,  
508 2003: The version-2 Global Precipitation Climatology Project (GPCP) monthly pre-  
509 cipitation analysis (1979-present). *J. Hydromet.*, **4**, 1147–1167.

510 Ammann, C. M., G. A. Meehl, W. M. Washington, and C. S. Zender, 2003: A monthly

- 511 and latitudinally varying volcanic forcing dataset in simulations of 20th century cli-  
512 mate. *Geophys. Res. Lett.*, **30**, 1657, doi:10.1029/2003GL016875.
- 513 Barth, M. C., P. J. Rasch, J. T. Kiehl, C. M. Benkovitz, and S. E. Schwartz, 2000:  
514 Sulfur chemistry in the National Center for Atmospheric Research Community Cli-  
515 mate Model: Description, evaluation, features and sensitivity to aqueous chemistry.  
516 *J. Geophys. Res.*, **105**, 1387–1415.
- 517 Bonan, G. B., K. W. Oleson, M. Vertenstein, S. Levis, X. Zeng, Y. Dai, R. E. Dickinson,  
518 and Z.-L. Yang, 2002: The land surface climatology of the Community Land Model  
519 coupled to the NCAR Community Climate Model. *J. Clim.*, **15**, 3123–3149.
- 520 Boville, B. A. and C. S. Bretherton, 2003: Heating and dissipation in the NCAR Com-  
521 munity Atmosphere Model. *J. Clim.*, **16**, 3877–3887.
- 522 Boville, B. A. and Etcetera, 2004: The impact of changing moist physical processes on  
523 the general circulation of CAM: Sensitivity studies. *J. Clim.*, *this issue*.
- 524 Boville, B. A. and P. R. Gent, 1998: The NCAR Climate System Model, Version One.  
525 *J. Clim.*, **11**, 1115–1130.
- 526 Boville, B. A., P. J. Rasch, and Etcetera, 2004: Effect of numerical formulation of FV  
527 atmospheric dynamics on the atmospheric general circulation. *J. Clim.*, *this issue*.
- 528 Briegleb, B. P., C. M. Bitz, E. C. Hunke, W. H. Lipscomb, M. M. Holland, J. L.  
529 Schramm, and R. E. Moritz, 2004: Scientific description of the sea ice compo-  
530 nent in the Community Climate System Model, Version Three. Technical Report  
531 NCAR/TN-463+STR, National Center for Atmospheric Research, Boulder, CO.  
532 80307-3000, 78 pp.
- 533 Cess, R. D., M. Zhang, B. A. Wielicki, D. F. Young, X.-L. Zhou, and Y. Nikitenko,  
534 2001: The influence of the 1998 El Niño upon cloud-radiative forcing over the Pa-  
535 cific warm pool. *J. Clim.*, **14**, 2129–2137.
- 536 Clough, S. A., F. X. Kneizys, and R. W. Davies, 1989: Line shape and the water vapor  
537 continuum. *Atmos. Res.*, **23**, 229–241.
- 538 Collins, W. D., 2001a: Effects of enhanced shortwave absorption on coupled simula-  
539 tions of the tropical climate system. *J. Clim.*, **14**, 1147–1165.
- 540 — 2001b: Parameterization of generalized cloud overlap for radiative calculations in  
541 general circulation models. *J. Atmos. Sci.*, **58**, 3224–3242.
- 542 Collins, W. D., C. M. Bitz, M. L. Blackmon, G. B. Bonan, C. S. Bretherton, J. A.  
543 Carton, P. Chang, S. C. Doney, J. J. Hack, T. H. Henderson, J. T. Kiehl, W. G. Large,  
544 D. S. McKenna, B. D. Santer, and R. D. Smith, 2004a: The Community Climate  
545 System Model, Version 3. *J. Clim.*, *this issue*.

- 546 Collins, W. D., J. K. Hackney, and D. P. Edwards, 2002a: A new parameterization  
547 for infrared emission and absorption by water vapor in the National Center for At-  
548 mospheric Research Community Atmosphere Model. *J. Geophys. Res.*, **107**, 8028,  
549 doi:10.1029/2000JD000032.
- 550 Collins, W. D., J. M. Lee-Taylor, D. P. Edwards, and G. L. Francis, 2004b: Effects of  
551 increased near-infrared absorption by water vapor on the climate system. *J. Geophys.*  
552 *Res.*, in preparation.
- 553 Collins, W. D., P. J. Rasch, B. A. Boville, J. J. Hack, J. R. McCaa, D. L. Williamson,  
554 J. T. Kiehl, B. Briegleb, C. Bitz, S.-J. Lin, M. Zhang, and Y. Dai, 2004c: De-  
555 scription of the NCAR Community Atmosphere Model (CAM3). Technical Report  
556 NCAR/TN-464+STR, National Center for Atmospheric Research, Boulder, Col-  
557 orado 80307-3000, 226 pp.
- 558 Collins, W. D., P. J. Rasch, B. E. Eaton, D. W. Fillmore, J. T. Kiehl, T. C. Beck,  
559 and C. S. Zender, 2002b: Simulation of aerosol distributions and radiative forc-  
560 ing for INDOEX: Regional climate impacts. *J. Geophys. Res.*, **107**, 4664, doi:  
561 10.1029/2001JD001365.
- 562 Collins, W. D., P. J. Rasch, B. E. Eaton, B. Khattatov, J.-F. Lamarque, and C. S. Zender,  
563 2001: Simulating aerosols using a chemical transport model with assimilation of  
564 satellite aerosol retrievals: Methodology for INDOEX. *J. Geophys. Res.*, **106**, 7313–  
565 7336.
- 566 Hack, J. J., C. M. Bitz, and Etcetera, 2004a: A slab ocean model. *J. Clim.*, *this issue*.
- 567 Hack, J. J., B. A. Boville, B. P. Briegleb, J. T. Kiehl, P. J. Rasch, and D. L. Williamson,  
568 1993: Description of the NCAR Community Climate Model (CCM2). Technical  
569 Report NCAR/TN-382+STR, National Center for Atmospheric Research, 120 pp.
- 570 Hack, J. J., A. G. Dai, and S. G. Yeager, 2004b: The hydrological cycle: Mean state.  
571 *J. Clim.*, *this issue*.
- 572 Hurrell, J. W. and Etcetera, 2004: Dynamic circulation and variability. *J. Clim.*, *this*  
573 *issue*.
- 574 Kållberg, P., A. Simmons, S. Uppala, and M. Fuentes, 2004: The ERA-40 archive.  
575 Technical Report ERA-40 Project Report No. 17, European Centre for Medium-  
576 Range Weather Forecasts, Reading, U.K., 35 pp.
- 577 Kiehl, J. T., 1998: Simulation of the tropical Pacific warm pool with the NCAR Climate  
578 System Model. *J. Clim.*, **11**, 1342–1355.
- 579 Kiehl, J. T. and P. R. Gent, 2003: The Community Climate System Model, Version  
580 Two. *J. Clim.*, **17**, 3666–3682.
- 581 Kiehl, J. T., J. Hack, G. Bonan, B. Boville, B. Briegleb, D. Williamson, and P. Rasch,  
582 1996: Description of the NCAR Community Climate Model (CCM3). Technical  
583 Report NCAR/TN-420+STR, National Center for Atmospheric Research, Boulder,  
584 Colorado, 152 pp.

- 585 Kiehl, J. T., J. J. Hack, G. B. Bonan, B. B. Boville, D. L. Williamson, and P. J. Rasch,  
586 1998: The National Center for Atmospheric Research Community Climate Model:  
587 CCM3. *J. Clim.*, **11**, 1131–1149.
- 588 King, M. D., W. P. Menzel, Y. J. Kaufman, D. Tanre, B. C. Gao, S. Platnick, S. A. Ack-  
589 erman, L. A. Remer, R. Pincus, and P. A. Hubanks, 2003: Cloud and aerosol prop-  
590 erties, precipitable water, and profiles of temperature and water vapor from MODIS.  
591 *IEEE Trans. Geosci. Remote Sens.*, **41**, 442–458.
- 592 Kistler, R., E. Kalnay, W. Collins, S. Saha, G. White, J. Woollen, M. Chelliah,  
593 W. Ebisuzaki, M. Kanamitsu, V. Kousky, H. van den Dool, R. Jenne, and M. Fior-  
594 ino, 2001: The NCEP-NCAR 50-year reanalysis: Monthly means CD-ROM and  
595 documentation. *Bull. Am. Meteorol. Soc.*, **82**, 247–267.
- 596 Kristjánsson, J. E. and J. Kristiansen, 2000: Impact of a new scheme for optical prop-  
597 erties of ice crystals on climates of two GCMs. *J. Geophys. Res.*, **105**, 10063–10079.
- 598 Large, W. G., G. Danabasoglu, and I. Wainer, 2004: Attribution and implications of  
599 upper ocean biases in CCSM3. *J. Clim.*, *this issue*.
- 600 Lawrence, M. G. and P. J. Crutzen, 1998: The impact of cloud particle gravitational  
601 settling on soluble trace gas distributions. *Tellus*, **50B**, 263–289.
- 602 Levis, S. and G. B. Bonan, 2004: Evaluation of CLM parameterizations and CAM-  
603 CLM climate using the CLM-DGVM as a diagnostic tool. *J. Clim.*, *this issue*.
- 604 Levis, S., G. B. Bonan, M. Vertenstein, and K. W. Oleson, 2004: The Community Land  
605 Model’s Dynamic Global Vegetation Model (CLM-DGVM): Technical description  
606 and user’s guide. Technical Report NCAR/TN-459+IA, National Center for Atmo-  
607 spheric Research, Boulder, CO. 80307-3000, 50 pp.
- 608 Lin, S.-J. and R. B. Rood, 1996: Multidimensional flux-form semi-Lagrangian trans-  
609 port schemes. *Mon. Wea. Rev.*, **124**, 2046–70.
- 610 Oleson, K. W., Y. Dai, G. B. Bonan, M. Bosilovich, R. Dickinson, P. Dirmeyer,  
611 F. Hoffman, P. Houser, S. Levis, G.-Y. Niu, P. Thornton, M. Vertenstein, Z.-L. Yang,  
612 and X. Zeng, 2004: Technical description of the Community Land Model (CLM).  
613 Technical Report NCAR/TN-461+STR, National Center for Atmospheric Research,  
614 Boulder, CO. 80307-3000, 174 pp.
- 615 Ramanathan, V., R. D. Cess, E. F. Harrison, P. Minnis, B. R. Barkstrom, E. Ahmad,  
616 and D. Hartmann, 1989: Cloud-radiative forcing and climate: Results from the Earth  
617 Radiation Budget Experiment. *Science*, **243**, 57–63.
- 618 Randel, D. L., T. H. V. Haar, M. A. Ringerud, G. Stephens, T. J. Greenwald, and  
619 C. L. Combs, 1996: A new global water vapor dataset. *Bull. Am. Meteorol. Soc.*, **77**,  
620 1233–1246.
- 621 Rasch, P. J., 2004: Characteristics of transport using three formulations of atmospheric  
622 dynamics in a single GCM framework. *J. Clim.*, *this issue*.

- 623 Rasch, P. J., M. C. Barth, J. T. Kiehl, S. E. Schwartz, and C. M. Benkovitz, 2000: A  
624 description of the global sulfur cycle and its controlling processes in the National  
625 Center for Atmospheric Research Community Climate Model, Version 3. *J. Geophys. Res.*, **105**, 1367–1385.  
626
- 627 Rasch, P. J., W. D. Collins, and B. E. Eaton, 2001: Understanding the Indian Ocean Ex-  
628 periment (INDOEX) aerosol distributions with an aerosol assimilation. *J. Geophys.*  
629 *Res.*, **106**, 7337–7356.
- 630 Rasch, P. J. and Etcetera, 2004: The hydrological cycle: Transients. *J. Clim.*, *this issue*.
- 631 Rasch, P. J. and J. E. Kristjánsson, 1998: A comparison of the CCM3 model climate  
632 using diagnosed and predicted condensate parameterizations. *J. Clim.*, **11**, 1587–  
633 1614.
- 634 Rossow, W. B. and R. A. Schiffer, 1999: Advances in understanding clouds from IS-  
635 CCP. *Bull. Am. Meteorol. Soc.*, **80**, 2261–2287.
- 636 Rothman, L. S., A. Barbe, D. C. Benner, L. R. Brown, C. Camy-Peyret, M. R. Carleer,  
637 K. Chance, C. Clerbaux, V. Dana, V. M. Devi, A. Fayt, J.-M. Flaud, R. R. Gamache,  
638 A. Goldman, D. Jacquemart, K. W. Jucks, W. J. Lafferty, J.-Y. Mandin, S. T.  
639 Massie, V. Nemtchinov, D. A. Newnham, A. Perrin, C. P. Rinsland, J. Schroeder,  
640 K. M. Smith, M. A. H. Smith, K. Tang, R. A. Toth, J. V. Auwera, P. Varanasi, and  
641 K. Yoshino, 2003: The HITRAN molecular spectroscopic database: Edition of 2000  
642 including updates of 2001. *J. Quant. Spectrosc. Radiat. Transfer*, **82**.
- 643 Sundqvist, H.: 1988, Parameterization of condensation and associated clouds in models  
644 for weather prediction and general circulation simulation. *Physically-based Mod-*  
645 *elling and Simulation of Climate and Climate Change*, M. E. Schlesinger, ed.,  
646 Kluwer Academic, volume 1, 433–461.
- 647 Waliser, D. E., W. D. Collins, and S. P. Anderson, 1996: An estimate of the surface  
648 shortwave cloud forcing over the western Pacific during TOGA COARE. *Geophys.*  
649 *Res. Lett.*, **23**, 519–522.
- 650 Washington, W. M., 1982: Documentation for the Community Climate Model (CCM),  
651 Version 0. Technical Report NTIS No. PB82 194192, National Center for Atmo-  
652 spheric Research, Boulder, Colorado.
- 653 Williamson, D. L., 1983: Description of NCAR Community Climate Model (CCM0B).  
654 Technical Report NCAR/TN-210+STR, National Center for Atmospheric Research,  
655 Boulder, Colorado, NTIS No. PB83 23106888, 88 pp.
- 656 Williamson, D. L.: 1995, Skill scores from the AMIP simulations. *Proceedings of the*  
657 *first International AMIP Scientific Conference*, W. L. Gates, ed., World Meteorolog-  
658 ical Organization, 253–256.
- 659 Williamson, D. L., 2002: Time-split versus process-split coupling of parameterizations  
660 and dynamical core. *Mon. Wea. Rev.*, **130**, 2024–2041.

- 661 Williamson, D. L., J. T. Kiehl, V. Ramanathan, R. E. Dickinson, and J. J. Hack,  
662 1987: Description of NCAR Community Climate Model (CCM1). Technical Report  
663 NCAR/TN-285+STR, National Center for Atmospheric Research, Boulder, Col-  
664 orado, 112 pp.
- 665 Zdunkowski, W. G., W.-G. Panhans, R. M. Welch, and G. J. Korb, 1982: A radiation  
666 scheme for circulation and climate models. *Contrib. Atmos. Phys.*, **55**, 215–238.
- 667 Zhang, M., W. Lin, C. B. Bretherton, J. J. Hack, and P. J. Rasch, 2003: A modified for-  
668 mulation of fractional stratiform condensation rate in the NCAR Community Atmo-  
669 sphere Model (CAM2). *J. Geophys. Res.*, **108**, 4035, doi:10.1029/2002JD002523.
- 670 Zhang, Y. C., W. B. Rossow, A. A. Lacis, V. Oinas, and M. I. Mishchenko, 2004:  
671 Calculation of radiative fluxes from the surface to top of atmosphere based on ISCCP  
672 and other global data sets: Refinements of the radiative transfer model and the input  
673 data. *J. Geophys. Res.*, **109**, D19105, doi:10.1029/2003JD004457.

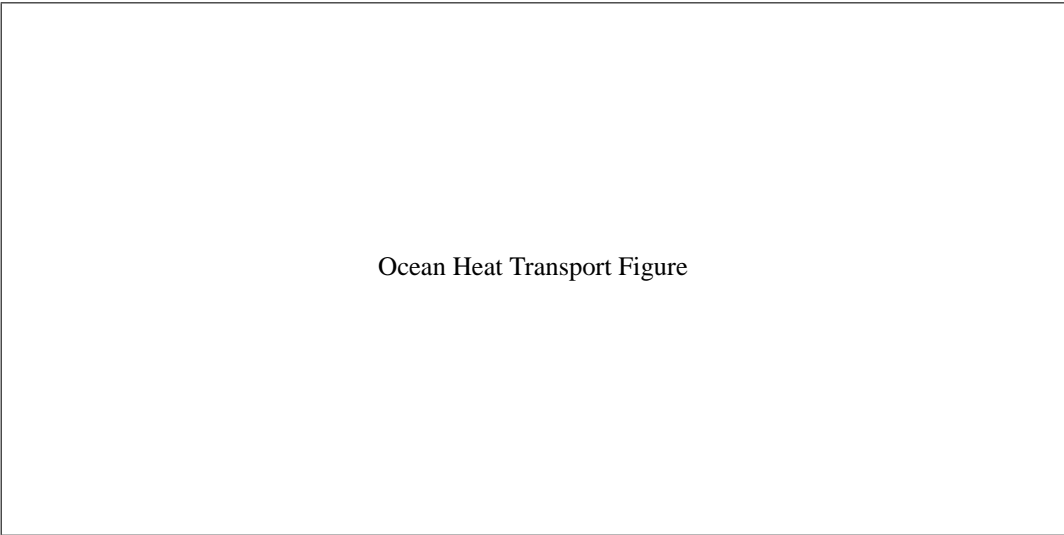


Figure 1: Difference in annual-mean meridional ocean heat transport between CAM2 and CAM3.



Figure 2: Zonal-mean surface precipitation. Panel A: Annually-averaged total surface precipitation from CAM2, CAM3, and GPCP; panel B: differences between the models and GPCP estimates.

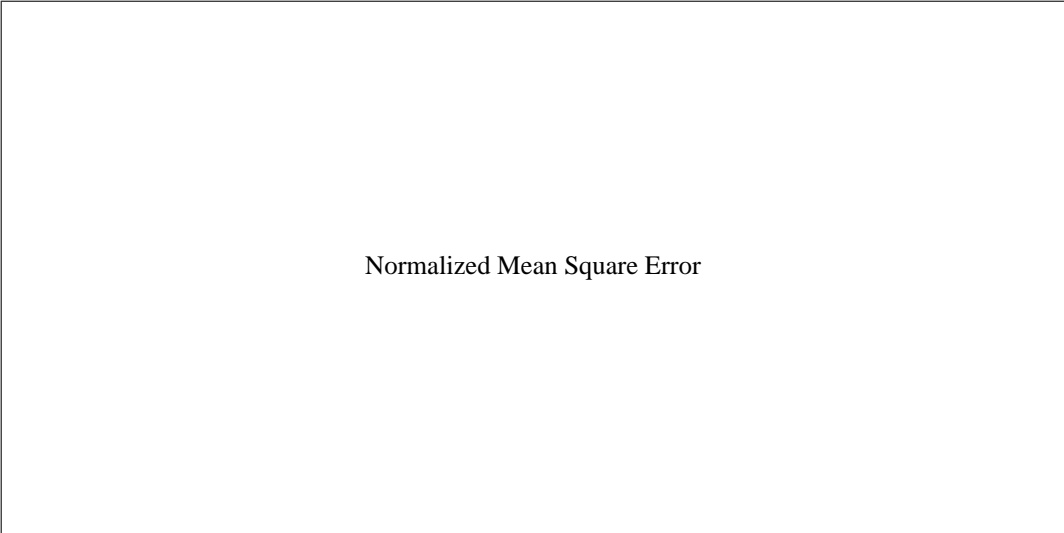


Figure 3: Normalized mean square error (NMSE) and scaled variance ratio (SVR) for the 200-mb height field. The bars are: green:  $U(z_m)$ , yellow:  $C(z_m)$ , red:  $P(z_m)$ , and blue:  $SVR(z_m)$ . The sum of the red, green, and yellow bars equals the  $NMSE(z_m)$ .

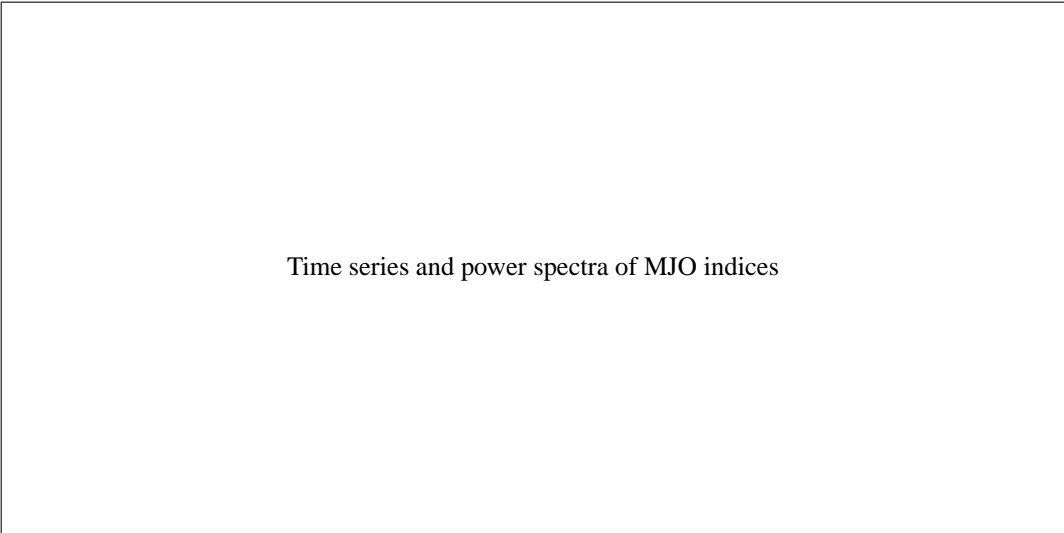


Figure 4: MJO indices for NCEP reanalysis and one member of the T85 CAM3 AMIP ensemble. Panel A: Time series of the indices; panel B: power spectra of the indices.